Published in final edited form as:
J Nucl Med. 2009 August ; 50(8): 1276–1282. doi:10.2967/jnumed.109.062265.

Initial Evaluation of ^{11}C-DPA-713, a Novel TSPO PET Ligand, in Humans

Christopher J. Endres[1], **Martin G. Pomper**[1], **Michelle James**[2], **Ovsev Uzuner**[1], **Dima A. Hammoud**[3], **Crystal C. Watkins**[1], **Aaron Reynolds**[4], **John Hilton**[1], **Robert F. Dannals**[1], and **Michael Kassiou**[2,4,5]

[1] Division of Neuroradiology, Johns Hopkins University, Baltimore, Maryland [2] Brain and Mind Research Institute, University of Sydney, Sydney, New South Wales, Australia [3] Radiology and Imaging Sciences, National Institutes of Health/Clinical Center, Bethesda, Maryland [4] School of Chemistry, University of Sydney, Sydney, New South Wales, Australia [5] Discipline of Medical Radiation Sciences, University of Sydney, Sydney, New South Wales, Australia

Abstract

Translocator protein (TSPO) is upregulated in activated microglia and thus can serve as a marker of neuroinflammation. Recently, a novel radioligand, ^{11}C-*N*,*N*-diethyl-2-[2-(4-methoxyphenyl)-5,7-dimethyl-pyrazolo[1,5-a]pyrimidin-3-yl]-acetamide (^{11}C-DPA-713), has been described that binds to TSPO with high affinity. Here, we report the first examination of ^{11}C-DPA-713 in human subjects using PET.

Methods—Five healthy controls were studied with PET for 90 min after a bolus injection of high-specific-activity ^{11}C-DPA-713. For comparison, 2 additional healthy controls were studied with ^{11}C-*R*-PK11195. Arterial blood sampling and metabolite analysis were performed to allow the accurate quantification of tracer kinetics. Tracer uptake was evaluated for several brain regions. Tissue time–activity curves were fitted using 1- and 2-tissue-compartment models, with goodness-of-fit tests showing a preference for the 2-tissue model.

Results—In the healthy brain, the average plasma-to-tissue clearance and the total volume of distribution were an order of magnitude larger than measured for ^{11}C-*R*-PK11195. Accordingly, dose-normalized time–activity curves showed that ^{11}C-DPA-713 gives a larger brain signal.

Conclusion—Studies in patient populations will help determine whether ^{11}C-DPA-713 provides better sensitivity for evaluating increased TSPO expression. This initial study in humans shows that ^{11}C-DPA-713 is a promising ligand for evaluating TSPO binding with PET.

Keywords

compartmental analysis; microglia; positron emission tomography; translocator protein

Microglia are the resident macrophages of the central nervous system (CNS), responsible for phagocytosis of cellular debris, antigen presentation, and a multitude of other functions in the CNS (1). Once exposed to neuronal injury, microglial cells become activated, with resultant phenotypic transformation from a ramified to an enlarged amoeboid morphology (2). When activated, microglia demonstrate increased expression of translocator protein (TSPO), previously known as the peripheral benzodiazepine receptor (PBR) (3), which is an 18-kDa

For correspondence or reprints contact: Christopher J. Endres, Division of Neuroradiology, Johns Hopkins University, 1550 Orleans St., CRB II Room 491, Baltimore, MD 21231. endres@jhmi.edu.

protein localized primarily to the outer mitochondrial membrane (4) of many cells. In the normal brain, TSPO expression has been described in endothelial and smooth muscle cells, subpial glia, intravascular monocytes, and ependymal cells (5). In view of the increased TSPO expression associated with activated microglia and macrophages in states of disease (5,6), TSPO is considered a marker of the neuroinflammatory burden.

Microglial activation is suspected in playing a role in the pathophysiology of multiple CNS diseases. Therefore, a reliable imaging biomarker for microglial activation could prove useful in better characterizing those diseases noninvasively. Unlike anatomic imaging techniques such as CT and MRI, functional imaging techniques, namely PET, can image microglial activation through the use of radioactively labeled ligands that bind to TSPO. The prototype of such radioligands is ^{11}C-*R*-PK11195, a lipid-soluble isoquinoline carboxamide, with the *R*-enantiomer having higher affinity for TSPO than the *S*-enantiomer (7). Despite being used extensively in the imaging of multiple CNS disease entities, ^{11}C-*R*-PK11195 suffers from many limitations including high nonspecific binding, high plasma protein binding, low brain uptake (8), and the lack of a universally validated compartmental model to describe the kinetic behavior in the brain across different pathologies (9–12). Those limitations have instigated the search for alternative TSPO binding radioligands with more favorable characteristics such as higher affinity, lower nonspecific binding, lower protein binding, and higher brain uptake. Numerous TSPO PET ligands have been developed in the last several years (13), including ^{11}C-DAA1106 (14) and ^{11}C-PBR28 (15).

Recently, a pyrazolopyrimidine, ^{11}C-*N*,*N*-diethyl-2-[2-(4-methoxyphenyl)-5,7-dimethyl-pyrazolo[1,5-a]pyrimidin-3-yl]-acetamide (^{11}C-DPA-713), has been described (8,16). In animal studies, ^{11}C-DPA-713, compared with ^{11}C-*R*-PK11195, demonstrated higher affinity for TSPO (K_i = 4.7 vs. 9.3 nM). ^{11}C-DPA-713 is also less lipophilic (logP = 2.4) than ^{11}C-*R*-PK11195 (logP = 3.4) (16), suggesting that ^{11}C-DPA-713 should exhibit less nonspecific binding in the brain and lower binding to plasma proteins. The high specificity of ^{11}C-DPA-713 binding in vivo was demonstrated in a primate via the potent blockade of brain uptake when PK11195 was delivered before ^{11}C-DPA-713 (16). That study also showed that flumazenil had no blocking effect; thus, ^{11}C-DPA-713 binds exclusively to TSPO and not central benzodiazepine receptors (16). Studies in a rat model of neurodegeneration have shown ^{11}C-DPA-713 to have greater specificity in discriminating between normal and lesioned brain than ^{11}C-*R*-PK11195 (17). As a first step to study its potential for clinical use, we examined the cerebral uptake of ^{11}C-DPA-713 in healthy human control subjects and compared its pharmacokinetics with those of ^{11}C-*R*-PK11195.

MATERIALS AND METHODS

Radiopharmaceutical Preparation

The study was performed under Investigational New Drug number 78,283. ^{11}C-DPA-713 was synthesized according to the method of Maeda et al. (14). Radiochemical purity was greater than 95%.

Human Subjects

Seven healthy volunteers participated in this study. Five healthy male volunteers (mean age ± SD, 34 ± 8 y; mean weight ± SD, 86 ± 15 kg) were studied with ^{11}C-DPA-713, and 1 man (age, 55 y; weight, 79 kg) and 1 woman (age, 25 y; weight, 59.1 kg) were studied with ^{11}C-*R*-PK11195. This study was approved by the Johns Hopkins Institutional Review Board. The following are inclusion criteria for the study: healthy volunteers had to be 18–75 y old; the results of screening laboratory tests obtained for subjects less than 7 d before the PET study had to be within normal limits for sex and age; a 12-lead echocardiogram (ECG) had to be

within normal limits less than 7 d before the PET study, with the subject agreeing to another ECG within 7 d after the study; participants had to have no contraindications to MRI, which included metallic implants or prostheses, prohibitive claustrophobia, and pacemakers; and for women of childbearing potential, a negative serum pregnancy test less than 7 d before the PET study had to be demonstrated. Exclusion criteria included current or past opportunistic CNS infection at entry; history or current evidence of schizophrenia; current severe affective disorder believed to explain the patient's cognitive impairment; history of chronic neurologic disorder, such as multiple sclerosis or epilepsy, or structural CNS abnormality such as stroke or arteriovenous malformation; history of head injury with loss of consciousness for over 1 h; or history of active substance abuse (drugs or alcohol).

Brain Imaging

MRI—All subjects underwent brain MRI performed using a 1.5-T Signa Advantage system (GE Healthcare) and a 3-dimensional spoiled gradient-recalled (SPGR) acquisition in the steady state with the following parameters: repetition time, 50 ms; echo time, 5 ms; flip angle, 45°; number of excitations, 1; field of view, 24 × 24 cm; slice thickness, 1.5 mm; and reconstruction matrix, 256 × 256, yielding an in-plane pixel size of 0.93 × 0.93 mm. MRI scans were used to identify regions of interest (ROIs) for the cerebellum, caudate, cerebral peduncles, globus pallidus, midbrain, pons, putamen, thalamus, dorsolateral prefrontal cortex, ventromedial prefrontal cortex, and insula. ROIs were then transferred to the dynamic PET data to generate tissue time–activity curves.

PET—A thermoplastic mask was fitted to each subject's face for immobilization and positioning of the head during scanning. PET images were acquired on a High Resolution Research Tomograph (HRRT) (CPS/CTI), head-only camera, with axial spatial resolution (full width at half maximum) of 2.4 mm and an in-plane resolution of 2.4–2.8 mm (18). This scanner acquired 207 simultaneous slices (1.22-mm thickness). The axial and transaxial fields of view were 24.0 and 31.2 cm, respectively. To calculate an attenuation correction for the emission scans, a 6-min transmission scan was obtained with a ^{137}Cs (γ-energy, 662 keV) source before radiotracer injection. The attenuation map obtained with ^{137}Cs was converted using a lookup table to estimate attenuation coefficients for 511-keV photons.

PET Image Acquisition Protocol—^{11}C-DPA-713 (689 ± 63 MBq; 145 ± 81 GBq/μmol) or ^{11}C-*R*-PK11195 (681 ± 8 MBq; 147 ± 23 GBq/μmol) was delivered via intravenous bolus injection. Dynamic PET studies with ^{11}C-DPA-713 consisted of a 22-frame protocol (3 × 20, 2 × 30, 2 × 60, 3 × 120, 8 × 300, and 4 × 600 s) with a total scan duration of 90 min. For ^{11}C-*R*-PK11195, the last 3 frames were omitted, which gave a 60-min, 19-frame protocol. PET scans were reconstructed using ordered-subsets expectation maximum reconstruction, in a 31 × 31 cm field of view and a 256 × 256 pixel matrix, with a pixel size of 1.2 × 1.2 mm. PET frames were corrected for radioactive decay to the initial PET frame.

Measurement of ^{11}C-DPA-713 in Blood—For measurement of the blood input function, 25–35 blood samples (1 mL) were drawn throughout the PET period. In addition, 7 or 8 large (4-mL) samples were collected at 3, 5, 10, 20, 30, 45, 60, and 90 min to characterize radiolabeled metabolites in plasma. Blood sampling times were recorded manually. For total radioactivity measurement, blood samples were centrifuged, and 0.5-mL plasma radioactivity was counted in a NaI well counter (CompuGamma CS; Wallac Oy) that was cross-calibrated with the PET scanner. The time difference between the start of the camera and the start of well counting was recorded and used to correct the blood data for radioactive decay to the start time of the PET scan. ^{11}C-DPA-713 metabolites were separated from the parent compound by column-switch high-performance liquid chromatography (19). The capture column contained Strata-X sorbent (Phenomenex), and the analytic column (Prodigy ODS-3; Phenomenex) was

eluted with 60% acetonitrile in 50 mM potassium phosphate buffer (pH 2.4) at a flow rate of 2 mL/min. Plasma samples were loaded onto the capture column in 8 M urea to eliminate protein binding of the analytes. The metabolite fractions (M_f) were fitted to $M_f(t) = at(b+t)$, where t is time and a and b are fitted parameters. To determine the input function, $M_f(t)$ was used to correct the total radioactivity for radioactive metabolites at all time points. The terminal plasma clearance rate was measured by applying a monoexponential fit to the input function from 20 to 60 min. The reason for fitting to 60 min only was to allow a direct comparison to the clearance of ^{11}C-*R*-PK11195, which we typically study for 60 min.

Plasma Free Fraction (f_P)—In 3 subjects, a 4-mL blood sample was taken before radiotracer injection to assay for plasma protein binding using Centrifree ultrafiltration units (Millipore).

PET Data Analysis—To correct for small head movements, the PET frames from 4 min until the end of the study were coregistered to an early mean image that was created by averaging the frames from 1.5 to 10 min. PET-to-PET coregistration was performed using the normalized mutual information method and the realign function in SPM2 (Wellcome Department of Cognitive Neurology). After the realignment of the image frames, a mean PET image (20–90 min) was used for MRI–PET coregistration. MRI scans were used to identify the ROIs. Regions were then transferred to the dynamic PET data to generate tissue time–activity curves. ANALYZE software (Mayo Foundation) was used for processing ROIs and time–activity curves. Several methods were applied to quantify radiotracer uptake using a blood input function, including 1- and 2-tissue-compartment models and the graphical method of Logan et al. (20). The primary outcome measure was the total distribution volume (V_T) (21). Compartmental model fitting included a blood volume term (fixed to 4%) to account for vascular radioactivity. The 1-tissue model has 2 rate constants (K_1, k_2) that were fitted to determine $V_T = K_1/k_2$. The 2-tissue model has 4 rate constants (K_1, k_2, k_3, k_4) that were fitted to determine $V_T = K_1/k_2(1 + k_3/k_4)$. With the Logan method, a bilinear form of the equation was used, with V_T computed using the transformed data from 30 to 90 min. To determine the effect of using a shorter scan duration, V_T was also computed with stopping times of 60, 70, and 80 min. Compartmental modeling was applied to all data (0–90 min) and was also applied using stopping times of 60, 70, and 80 min. For each method of analysis, the parameter estimates obtained using a 90-min stopping time were taken as the standard estimates. For shorter stopping times, the percentage absolute difference from the standard estimates was calculated. For comparing relative tissue kinetics, 2 healthy control subjects were studied with ^{11}C-*R*-PK11195. As with ^{11}C-DPA-713, the ^{11}C-*R*-PK11195 studies were performed on the HRRT, with arterial sampling. On the basis of our existing protocol (22), the scan duration for ^{11}C-*R*-PK11195 studies was 60 min, and quantitative analysis was performed using the 1-tissue model to estimate K_1 and V_T.

RESULTS

Pharmacologic Effects

No pharmacologic effects were noted. All blood tests obtained before and after the scan were reviewed, and no abnormalities or interval changes were documented. All 12-lead ECGs obtained within 1 wk before and after DPA-713 injection were reviewed, and no abnormalities or interval changes were documented. Testing also included electrolyte panel, hepatic function panel, prothrombin time, heme-8 with differential, urea, creatinine, and glomerular filtration rate. No side effects were reported by any of the patients after the PET scans.

Plasma Analysis

The formation of blood metabolites was relatively slow. In particular, the plasma radioactivity after ^{11}C-DPA-713 consisted of only 20% metabolites at 30 min after injection, as compared with 40% metabolites for ^{11}C-*R*-PK11195 (Fig. 1). Although the dose-normalized ^{11}C-DPA-713 plasma concentration was lower than that measured for ^{11}C-*R*-PK11195, the terminal plasma clearance rates, as determined by monoexponential fitting from 20 to 60 min, were similar, with plasma clearance time constants of 42 and 37 min for ^{11}C-DPA-713 and ^{11}C-*R*-PK11195, respectively (Fig. 2). The f_P for ^{11}C-DPA-713 was 9.0% ± 2.6%, and for ^{11}C-*R*-PK11195 it was 1%.

Measurement of V_T

^{11}C-DPA-713 was taken up throughout the brain (Fig. 3), and the dose-normalized uptake was up to 3 times greater than was obtained with ^{11}C-*R*-PK11195 (Fig. 4). As judged by F test and the Akaike information criterion (23), ^{11}C-DPA-713 time–activity curves were better fit to a 2-tissue model than a 1-tissue model (Fig. 5). Although both models gave similar parameter estimates, the 2-tissue model tended to produce slightly higher V_T values than did the 1-tissue model. The coefficient of variation (COV) of V_T was similar for both models, but COV for K_1 was notably smaller with the 1-tissue model (5% on average) than with the 2-tissue model (15%). The finding that a 2-tissue model is preferred indicates that the assumption of rapid equilibrium among tissue compartments is violated, perhaps by the presence of a slowly clearing, nonspecific binding component, or within-region tissue heterogeneity. As compared with ^{11}C-*R*-PK11195, the ^{11}C-DPA-713 K_1 and V_T values were larger by an order of magnitude (Table 1).

Effect of Study Duration

Compared with V_T values obtained with the 2-tissue model using a full 90-min study, there was an average absolute difference of 2.8%, 3.6%, and 6.4% for study durations of 80, 70, and 60 minutes, respectively. For the Logan method, the differences were 2.2%, 4.2%, and 7.4%, respectively. In comparing the V_T values estimated with compartmental modeling and the Logan method, the absolute percentage differences were 4.9%, 5.0%, 6.5%, and 10% for stopping times of 90, 80, 70, and 60 min, respectively. In most cases, using an early stopping time led to an underestimation of V_T relative to the estimate obtained with a full 90-min dataset. Using scan durations of 50 min or less gave parameter estimates that were off by more than 10% on average.

DISCUSSION

Currently, there is increasing interest in the study of neuroinflammation. Because of the significance of TSPO as an effective marker of neuroinflammation, along with the general dissatisfaction with the pharmacokinetic properties of ^{11}C-*R*-PK11195, there has been a substantial effort to develop a TSPO ligand that has more favorable characteristics for PET (13). Aside from ^{11}C-DPA-713, two ligands that are of particular interest are ^{11}C-DAA1106 (14) and ^{11}C-PBR28 (15). A comparison of kinetic properties of these ligands is shown in Table 2. All 3 alternative ligands show a V_T that is an order of magnitude larger relative to ^{11}C-*R*-PK11195. Some of the increased uptake can be attributed to tracer delivery because ^{11}C-*R*-PK11195 has the smallest K_1 value. Both ^{11}C-DPA-713 and ^{11}C-PBR28 show much higher K_1, with ^{11}C-DAA1106 having a slightly higher K_1 value than ^{11}C-*R*-PK11195. The K_1 values also appear to be consistent with the f_P. Although f_P has not been reported for ^{11}C-DAA1106, it is presumably similar to that of ^{11}C-*R*-PK11195 given their similar calculated log of the octanol-to-water partition coefficient values. Note that the relative measured K_1 values will be nearly proportional to their respective f_P values if each ligand has a similar permeability surface area (PS) product (Appendix). When considering the normalized

tissue uptake (percentage standardized uptake value [%SUV]), ^{11}C-DPA-713 is greater than ^{11}C-PBR28 (15), which is greater than ^{11}C-*R*-PK11195; thus, the rank order of f_P, K_1, and %SUV is consistent for those 3 ligands. Some of the increased uptake is also likely due to specific binding because ^{11}C-*R*-PK11195 has the lowest affinity of the ligands shown in Table 2. However, for ^{11}C-DPA-713 and ^{11}C-PBR28, the affinity relative to ^{11}C-*R*-PK11195 is only marginally higher. Conversely, the V_T of ^{11}C-DAA1106 likely reflects greater specific binding as suggested by its much higher binding affinity. However, ^{11}C-DA1106 also has poor penetration (low K_1); thus, despite its high affinity, ^{11}C-DA1106 has V_T values comparable to those of ^{11}C-DPA-713 and ^{11}C-PBR28.

Here, in a direct comparison of ^{11}C-DPA-713 and ^{11}C-*R*-PK11195, we have shown ^{11}C-DPA-713 to have much greater normalized uptake (%SUV), which appears to be accounted for primarily by greater blood-to-brain delivery because both K_1 and V_T were an order of magnitude larger for ^{11}C-DPA-713. As explained in the Appendix, the differences in K_1, and therefore V_T, can be explained potentially by the difference in f_P between ^{11}C-*R*-PK11195 (1%) and ^{11}C-DPA-713 (9%). The accuracy of estimating f_P via micropore filtering of compounds that are highly lipophilic, such as ^{11}C-*R*-PK11195 and ^{11}C-DAA1106, is questionable and is likely why f_P is generally not reported for those compounds. However, it is clear that f_P is low for ^{11}C-*R*-PK11195; thus, at the very least our data indicate that ^{11}C-DPA-713 has a larger f_P that is also consistent with its higher brain uptake. The K_1 value for ^{11}C-*R*-PK11195 is relatively low, whereas the K_1 value for ^{11}C-DPA-713 is more comparable to that measured for other successful brain imaging agents (24–28). In this initial study of control subjects who presumably have minimal glial activity, and thus minimal TSPO binding, we cannot state definitively that ^{11}C-DPA-713 will show better specific uptake and superior sensitivity to ^{11}C-*R*-PK11195 for the assessment of glial activity in the human brain. However, the previous demonstration of highly specific uptake in the baboon brain (16), the better discrimination obtained with ^{11}C-DPA-713 in lesioned rat brain (17), and the higher affinity of ^{11}C-DPA-713 for TSPO (4.7 nM), as compared with ^{11}C-*R*-PK11195 (9.3 nM), suggest strongly that ^{11}C-DPA-713 has the potential to be a more sensitive imaging agent for evaluating TSPO binding.

CONCLUSION

In a healthy control population, ^{11}C-DPA-713 has excellent brain uptake and provides a higher brain signal than ^{11}C-*R*-PK11195. However, the evaluation of ^{11}C-DPA-713 uptake in patients with neuroinflammation will be needed to demonstrate more conclusively if this radioligand can provide better regional discrimination of brain injury than can ^{11}C-*R*-PK11195.

Acknowledgments

We appreciate the contribution of our research coordinators Rena Geckle and Priscilla Matthews for recruiting subjects, screening, and organizing subject records. This study is supported by a grant from The Dana Foundation (to M.G.P.) and the NIMH Toxicological Evaluation of Novel Ligands Program.

References

1. Raivich G. Like cops on the beat: the active role of resting microglia. Trends Neurosci 2005;28:571–573. [PubMed: 16165228]
2. Kreutzberg GW. Microglia: a sensor for pathological events in the CNS. Trends Neurosci 1996;19:312–318. [PubMed: 8843599]
3. Banati RB, Egensperger R, Maassen A, Hager G, Kreutzberg GW, Graeber MB. Mitochondria in activated microglia in vitro. J Neurocytol 2004;33:535–541. [PubMed: 15906160]

4. Papadopoulos V, Baraldi M, Guilarte TR, et al. Translocator protein (18kDa): new nomenclature for the peripheral-type benzodiazepine receptor based on its structure and molecular function. Trends Pharmacol Sci 2006;27:402–409. [PubMed: 16822554]
5. Cosenza-Nashat M, Zhao ML, Suh HS, et al. Expression of the translocator protein of 18 kDa by microglia, macrophages and astrocytes based on immunohistochemical localization in abnormal human brain. Neuropathol Appl Neurobiol 2009;35:306–328. [PubMed: 19077109]
6. Banati RB, Myers R, Kreutzberg GW. PK ('peripheral benzodiazepine')–binding sites in the CNS indicate early and discrete brain lesions: microautoradiographic detection of [^{3}H]PK11195 binding to activated microglia. J Neurocytol 1997;26:77–82. [PubMed: 9181482]
7. Shah F, Hume SP, Pike VW, Ashworth S, McDermott J. Synthesis of the enantiomers of [*N*-methyl-^{11}C]PK 11195 and comparison of their behaviours as radioligands for PK binding sites in rats. Nucl Med Biol 1994;21:573–581. [PubMed: 9234314]
8. Boutin H, Chauveau F, Thominiaux C, et al. In vivo imaging of brain lesions with [^{11}C]CLINME, a new PET radioligand of peripheral benzodiazepine receptors. Glia 2007;55:1459–1468. [PubMed: 17680643]
9. Kropholler MA, Boellaard R, Schuitemaker A, Folkersma H, van Berckel BN, Lammertsma AA. Evaluation of reference tissue models for the analysis of [^{11}C](*R*)-PK11195 studies. J Cereb Blood Flow Metab 2006;26:1431–1441. [PubMed: 16511500]
10. Kropholler MA, Boellaard R, Schuitemaker A, et al. Development of a tracer kinetic plasma input model for (*R*)-[^{11}C]PK11195 brain studies. J Cereb Blood Flow Metab 2005;25:842–851. [PubMed: 15744248]
11. Schuitemaker A, van Berckel BN, Kropholler MA, et al. Evaluation of methods for generating parametric (*R*)-[^{11}C]PK11195 binding images. J Cereb Blood Flow Metab 2007;27:1603–1615. [PubMed: 17311080]
12. Turkheimer FE, Edison P, Pavese N, et al. Reference and target region modeling of [^{11}C]-(*R*)-PK11195 brain studies. J Nucl Med 2007;48:158–167. [PubMed: 17204713]
13. Chauveau F, Boutin H, Van Camp N, Dolle F, Tavitian B. Nuclear imaging of neuroinflammation: a comprehensive review of [^{11}C]PK11195 challengers. Eur J Nucl Med Mol Imaging 2008;35:2304–2319. [PubMed: 18828015]
14. Maeda J, Suhara T, Zhang MR, et al. Novel peripheral benzodiazepine receptor ligand [^{11}C]DAA1106 for PET: an imaging tool for glial cells in the brain. Synapse 2004;52:283–291. [PubMed: 15103694]
15. Fujita M, Imaizumi M, Zoghbi SS, et al. Kinetic analysis in healthy humans of a novel positron emission tomography radioligand to image the peripheral benzodiazepine receptor, a potential biomarker for inflammation. Neuroimage 2008;40:43–52. [PubMed: 18093844]
16. James ML, Fulton RR, Henderson DJ, et al. Synthesis and in vivo evaluation of a novel peripheral benzodiazepine receptor PET radioligand. Bioorg Med Chem 2005;13:6188–6194. [PubMed: 16039131]
17. Boutin H, Chauveau F, Thominiaux C, et al. ^{11}C-DPA-713: a novel peripheral benzodiazepine receptor PET ligand for in vivo imaging of neuroinflammation. J Nucl Med 2007;48:573–581. [PubMed: 17401094]
18. Eriksson L, Wienhard K, Eriksson M, et al. The ECAT HRRT: NEMA NEC evaluation of the HRRT system, the new high-resolution research tomograph. IEEE Trans Nucl Sci 2002;49:2085–2088.
19. Hilton J, Yokoi F, Dannals RF, Ravert HT, Szabo Z, Wong DF. Column-switching HPLC for the analysis of plasma in PET imaging studies. Nucl Med Biol 2000;27:627–630. [PubMed: 11056380]
20. Logan J, Fowler JS, Volkow ND, et al. Graphical analysis of reversible radioligand binding from time-activity measurements applied to [*N*-^{11}C-methyl](−)-cocaine PET studies in human subjects. J Cereb Blood Flow Metab 1990;10:740–747. [PubMed: 2384545]
21. Innis RB, Cunningham VJ, Delforge J, et al. Consensus nomenclature for in vivo imaging of reversibly binding radioligands. J Cereb Blood Flow Metab 2007;27:1533–1539. [PubMed: 17519979]
22. Hammoud DA, Endres CJ, Chander AR, et al. Imaging glial cell activation with [^{11}C]-R-PK11195 in patients with AIDS. J Neurovirol 2005;11:346–355. [PubMed: 16162478]
23. Akaike H. A new look at the statistical model identification. IEEE Trans Automat Contr 1974;19:716–723.

24. Buck A, Gucker PM, Schonbachler RD, et al. Evaluation of serotonergic transporters using PET and [^{11}C](+)McN-5652: assessment of methods. J Cereb Blood Flow Metab 2000;20:253–262. [PubMed: 10698061]
25. Endres CJ, Bencherif B, Hilton J, Madar I, Frost JJ. Quantification of brain μ-opioid receptors with [^{11}C]carfentanil: reference-tissue methods. Nucl Med Biol 2003;30:177–186. [PubMed: 12623117]
26. Ginovart N, Willeit M, Rusjan P, et al. Positron emission tomography quantification of [^{11}C]-(+)-PHNO binding in the human brain. J Cereb Blood Flow Metab 2007;27:857–871. [PubMed: 17033687]
27. Koeppe RA, Frey KA, Snyder SE, Meyer P, Kilbourn MR, Kuhl DE. Kinetic modeling of *N*-[^{11}C] methylpiperidin-4-yl propionate: alternatives for analysis of an irreversible positron emission tomography trace for measurement of acetylcholinesterase activity in human brain. J Cereb Blood Flow Metab 1999;19:1150–1163. [PubMed: 10532640]
28. Treyer V, Streffer J, Wyss MT, et al. Evaluation of the metabotropic glutamate receptor subtype 5 using PET and ^{11}C-ABP688: assessment of methods. J Nucl Med 2007;48:1207–1215. [PubMed: 17574984]
29. Koeppe RA, Holthoff VA, Frey KA, Kilbourn MR, Kuhl DE. Compartmental analysis of [^{11}C] flumazenil kinetics for the estimation of ligand transport rate and receptor distribution using positron emission tomography. J Cereb Blood Flow Metab 1991;11:735–744. [PubMed: 1651944]
30. Selleri S, Bruni F, Costagli C, et al. 2-Arylpyrazolo[1,5-a]pyrimidin-3-yl acetamides: new potent and selective peripheral benzodiazepine receptor ligands. Bioorg Med Chem 2001;9:2661–2671. [PubMed: 11557354]
31. Briard E, Zoghbi SS, Imaizumi M, et al. Synthesis and evaluation in monkey of two sensitive ^{11}C-labeled aryloxyanilide ligands for imaging brain peripheral benzodiazepine receptors in vivo. J Med Chem 2008;51:17–30. [PubMed: 18067245]
32. Ikoma Y, Yasuno F, Ito H, et al. Quantitative analysis for estimating binding potential of the peripheral benzodiazepine receptor with [^{11}C]DAA1106. J Cereb Blood Flow Metab 2007;27:173–184. [PubMed: 16685259]

APPENDIX

Consider an ideal case in which plasma radiotracer is entirely in a free state (i.e., with no tracer binding to plasma protein). We can define a free plasma compartment that is characterized by concentration C_{FP}, where C_{FP} is a standardized term for tracer that is free in plasma (21). The unidirectional tracer flux (dC^U_{FP}/dt) leaving the compartment (e.g., via clearance into surrounding tissue) is given by

$$dC^U_{FP}/dt = K^0_1 C_{FP}, \qquad \text{Eq. 1A}$$

where K^0_1 is a first-order rate constant that can be considered the baseline or true clearance rate when all tracer is freely available for transport. If we assume that a component of the tracer plasma concentration is bound, for example, to protein, but that the bound component is in rapid equilibrium with free tracer, then we can define $C_{FP} = f_P C_P$ (Eq. 9 from Innis et al. (21)), where C_P is the total (free + bound) plasma concentration, and f_P is the plasma free fraction. Analogous to Equation 1A, we can then define the unidirectional flux of tracer from the total plasma compartment as

$$dC^U_P/dt = K_1 C_P. \qquad \text{Eq. 2A}$$

In typical modeling applications, the total plasma concentration is taken as the input function, and thus the fitted delivery rate constant is K_1. By definition, tracer that is bound cannot contribute directly to the tracer flux because the tracer must first become unbound before it can be delivered elsewhere. Thus the total tracer flux (Eq. 2A) is equivalent to the free tracer flux (Eq. 1A), which gives

$$K_1^0 C_{FP} = K_1 C_P. \quad \text{Eq. 3A}$$

Because $C_{FP} = f_P C_P$, we find that the value of K_1 is proportional to f_P (Eq. 4A).

$$K_1 = f_P K_1^0. \quad \text{Eq. 4A}$$

Equation 4A is analogous to the effect of tissue nonspecific binding on rate constants that originate in the tissue free compartment (29). The dependency of K_1 on f_P is evident in the comparison of TSPO ligands in Table 2. However, in comparing K_1 for different ligands, Equation 4A will strictly hold only when K_1^0 is equivalent for all ligands. That is unlikely given that K_1^0 is also affected by the permeability surface area (PS) product, which will be unique for each ligand. However, if there is not too much variability in PS, then f_P is a useful measure for predicting relative K_1 values.

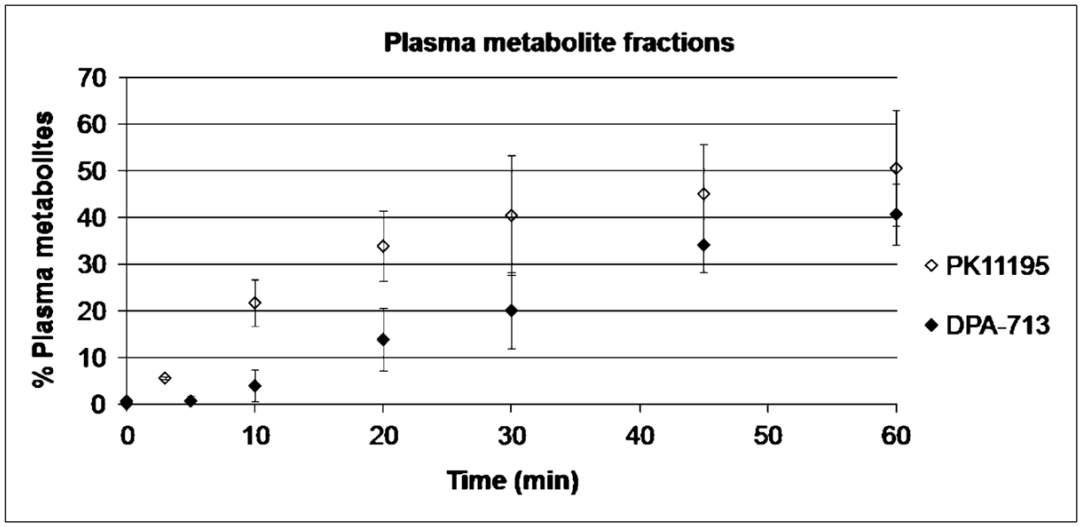

FIGURE 1.
Plasma metabolites for ^{11}C-DPA-713 and ^{11}C-*R*-PK11195 in human subjects. Plot shows mean and SD for ^{11}C-DPA-713 (n = 5) and ^{11}C-*R*-PK11195 (n = 2).

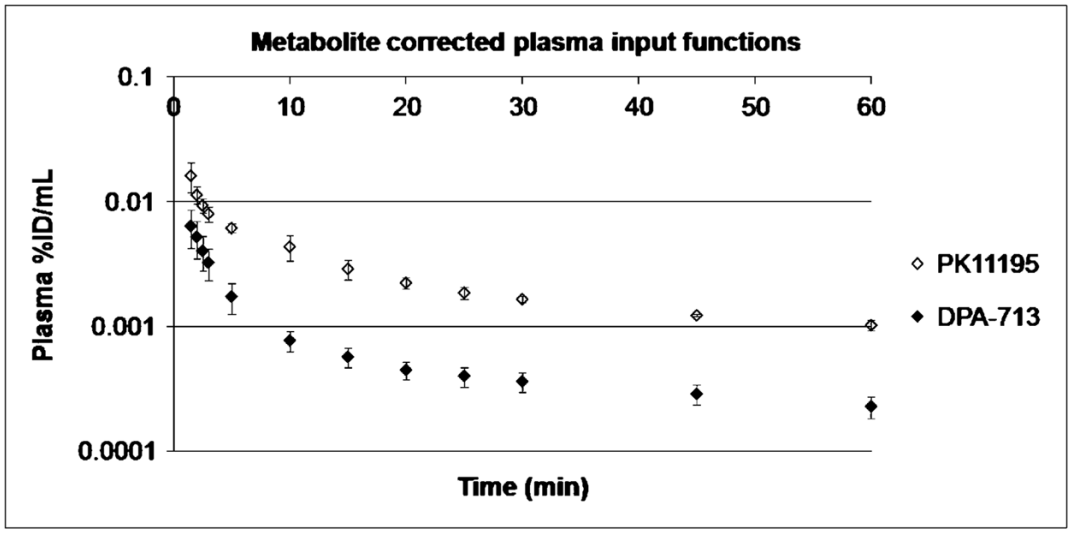

FIGURE 2.
Metabolite-corrected plasma input functions in human subjects. Plot shows mean and SD for ^{11}C-DPA-713 (*n* = 5) and ^{11}C-*R*-PK11195 (*n* = 2). %ID/mL = dose-normalized uptake.

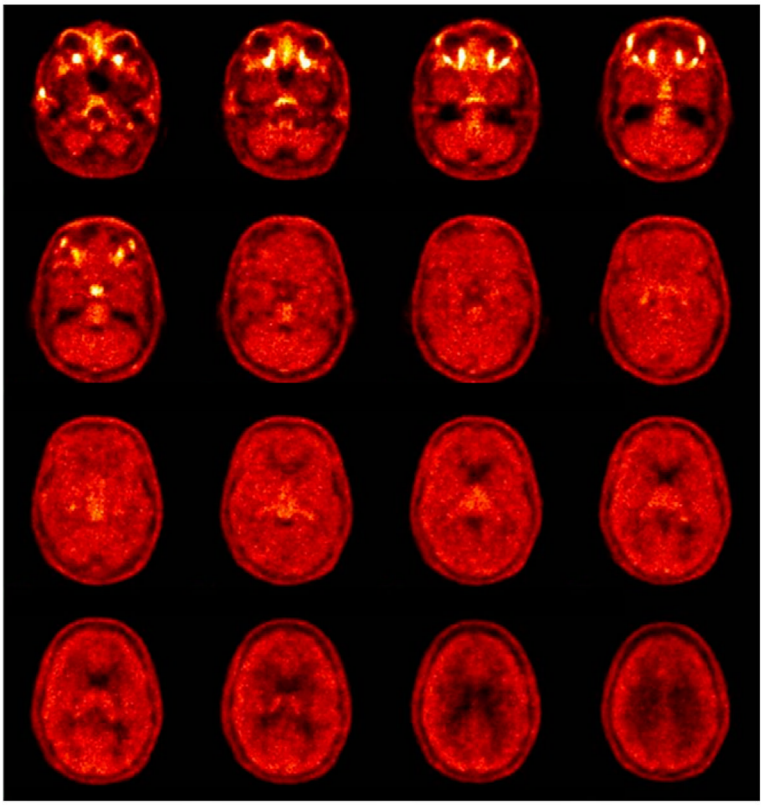

FIGURE 3.
Brain radioactivity distribution after bolus injection of ^{11}C-DPA-713 in healthy male control. Images have been averaged from 20 to 90 min after injection.

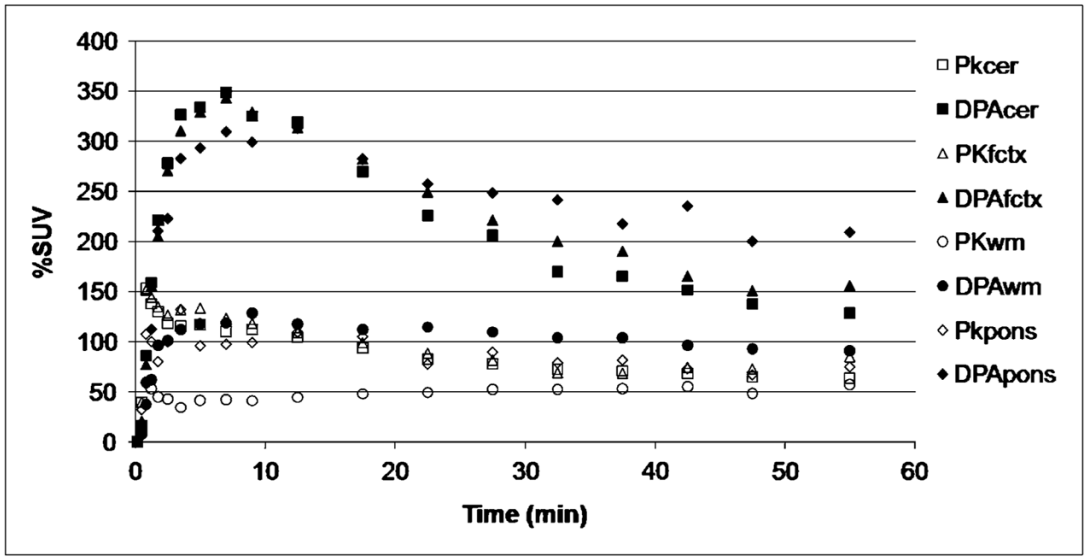

FIGURE 4.

Comparison of radiotracer time–activity curves (mean %SUV) of ^{11}C-DPA-713 (n = 5) and ^{11}C-*R*-PK11195 (n = 2) in cerebellum (cer), frontal cortex (fctx), white matter (wm), and pons.

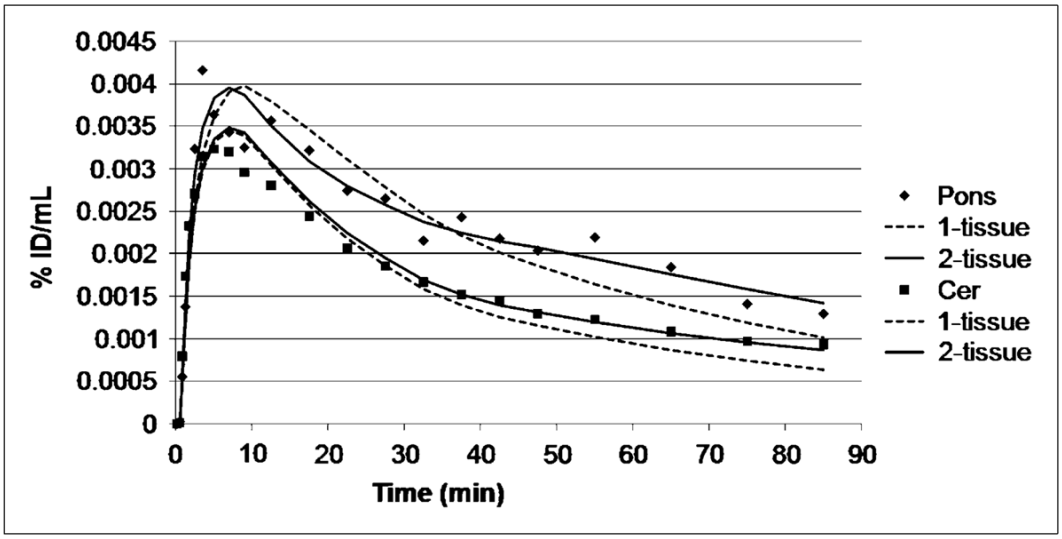

FIGURE 5.
^{11}C-DPA-713 time–activity curves in pons and cerebellum (cer) fitted to 1- and 2-tissue-compartment models.

TABLE 1

Comparison of K_1 and V_T Estimates Obtained from 1-Tissue Model for ^{11}C-DPA-713 ($n = 5$) and ^{11}C-*R*-PK11195 ($n = 2$)

	K_1 value		V_T value	
ROI	**DPA-713**	**PK11195**	**DPA-713**	**PK11195**
Caudate	0.25 ± 0.05 (4.0)	0.020 ± 0.012 (24.9)	3.08 ± 0.57 (3.8)	0.25 ± 0.09 (23.1)
Cerebellar cortex	0.27 ± 0.03 (4.8)	0.025 ± 0.016 (12.5)	3.88 ± 0.85 (4.5)	0.32 ± 0.08 (11.9)
Frontal	0.27 ± 0.05 (4.3)	0.023 ± 0.013 (14.6)	4.11 ± 0.84 (4.1)	0.33 ± 0.10 (13.9)
Pons	0.20 ± 0.07 (5.4)	0.019 ± 0.016 (23.1)	5.06 ± 0.83 (5.5)	0.42 ± 0.13 (33.3)
Putamen	0.29 ± 0.06 (4.8)	0.026 ± 0.015 (10.3)	3.54 ± 0.56 (4.5)	0.34 ± 0.06 (9.5)
Temporal	0.23 ± 0.04 (4.5)	0.016 ± 0.011 (22.0)	3.69 ± 0.69 (4.3)	0.40 ± 0.08 (29.4)
Thalamus	0.27 ± 0.04 (5.0)	0.025 ± 0.013 (12.0)	4.72 ± 0.90 (4.8)	0.42 ± 0.07 (11.9)

Data are mean ± SD. Mean COV (percentage standard fitting error) is shown in parentheses.

TABLE 2

Comparison of Pharmacokinetic Properties of 4 TSPO Ligands, Including Kinetic Parameters Measured in Human Subjects

Ligand	cLogP	f_P (%)	K_i/(PK11195 K_i)	K_1 (mL/cm^3/min)	V_T (mL/cm^3)
^{11}C-*R*-PK11195	5.11	1.0	1	0.016–0.026	0.25–0.42
^{11}C-DPA-713	2.63	9.0	0.5 (30)	0.20–0.29	3.1–5.1
^{11}C-PBR28	3.29	3.3 (15)	0.22–0.93 (31)	0.10–0.14 (15)	3.3–4.6 (15)
^{11}C-DAA1106	4.38	ND	0.053–0.099 (31)	0.048–0.066 (32)	3.8–5.0 (32)

cLogP = calculated log of octanol-to-water partition coefficient; ND = not determined.

Range of K_1 values represents measurements obtained in different tissue regions. Values of K_i/(PK11195 K_i) are ratio of K_i of ligand to K_i of PK11195 and are taken from measurements in mitochondrial tissue. Range of K_i ratios represents values taken from different species including rat, monkey, and human. For ^{11}C-DPA-713, ratio was measured with rat mitochondria only. Values that do not have reference were determined in present study. cLogP was computed with ACD/PhysChem Suite (Advanced Chemistry Development).

J Nucl Med. Author manuscript; available in PMC 2010 June 10.